Yonago Acta Medica 2023;66(1):7–18 doi: 10.33160/yam.2023.02.002

Comparison of Characterization in Two-Dimensional and Three-Dimensional Canine Mammary Gland Tumor Cell Models

Tomohiro Osaki,* Yuji Sunden,* Katsuhiko Warita* and Yoshiharu Okamoto*
**Joint Department of Veterinary Medicine, Faculty of Agriculture, Tottori University, Tottori 680-8553, Japan*

ABSTRACT

Background Canine mammary gland tumors can be used as predictive models for human breast cancer. There are several types of microRNAs common in human breast cancer and canine mammary gland tumors. The functions of microRNAs in canine mammary gland tumors are not well understood.

Methods We compared the characterization of microRNA expression in two-dimensional and three-dimensional canine mammary gland tumor cell models. We evaluated the differences between two- and three-dimensional cultured canine mammary gland tumor SNP cells by assessing microRNA expression levels, morphology, drug sensitivity, and hypoxia.

Results The expression of microRNA-210 in the three-dimensional-SNP cells was 10.19 times higher than that in the two-dimensional-SNP cells. The intracellular concentrations of doxorubicin in the two- and three-dimensional-SNP cells were 0.330 ± 0.013 and 0.290 ± 0.048 nM/mg protein, respectively. The IC_{50} values of doxorubicin for the two- and three-dimensional-SNP cells were 5.2 and 1.6 μM, respectively. Fluorescence of the hypoxia probe, LOX-1, was observed inside the sphere of three-dimensional-SNP cells without echinomycin but not in two-dimensional-SNP cells. The three-dimensional-SNP cells treated with echinomycin showed weak LOX-1 fluorescence.

Conclusion The present study showed a clear difference in microRNA expression levels in cells cultured in a two-dimensional adherent versus a three-dimensional spheroid model.

Key words canine; mammary gland tumor; microRNA; three-dimensional; two-dimensional

Canine mammary gland tumors (CMGTs), which account for 50% of all canine tumors, are the most commonly diagnosed cancer in sexually intact female dogs.[1, 2] Surgery is the primary treatment for CMGTs. However, the combination of chemotherapy and/or radiotherapy has not been shown to be sufficiently effective compared to surgery alone in dogs.[1, 3]

Recently, dogs have become excellent targets for comparative oncology, and CMGTs have been used as predictive models for human breast cancer.[2] Some studies have focused on microRNAs (miRNAs). miRNAs are small, single-stranded RNAs that act as post-transcriptional repressors of gene expression.[4] Several types of miRNAs have been identified in human breast cancer[5–7] and CMGTs.[8–10] In some in vitro studies, cells were cultured as monolayers on flat surfaces in dishes or flasks and used for miRNA expression analysis.[11, 12] However, these culture conditions do not accurately reflect the biological environment.

The most commonly used type of cell culture is the adherent two-dimensional (2D) monolayer culture model; however, three-dimensional (3D) spheroid cultures have been recently developed for cancer research.[13] Although 2D monolayer cultures provide a convenient means of treating and analyzing cells, limitations associated with 2D models have been identified.[13] In the 2D model, cell-to-cell and cell-to-extracellular matrix (ECM) interactions are not represented as they are in the tumor mass.[13] In contrast, 3D models simulate a histopathological cellular microenvironment in a tumor, reconstruct a tissue-like cytoarchitecture with cell-to-cell and cell-to-ECM interactions, and exhibit growth, differentiation, and therapeutic responses, such as in vivo.[14] In our previous study, we established that SNP cells from a CMGT were characterized by proliferation in a tubulopapillary pattern and mesenchymal transition.[15] In this study, we established a 3D in vitro cell culture model for SNP cells.

To the best of our knowledge, there have been a few reports on miRNA expression in CMGTs. Therefore, the function of miRNAs in CMGTs is not well understood. In the present study, we evaluated the differences between 2D- and 3D-cultured CMGTs by assessing their morphology, drug sensitivity, hypoxia, and miRNA expression levels.

Corresponding author: Tomohiro Osaki, DVM, PhD
tosaki@tottori-u.ac.jp
Received 2022 October 13
Accepted 2022 November 28
Online published 2023 February 20
Abbreviations: CMGTs, canine mammary gland tumors; ECM, extracellular matrix; miRNAs, microRNAs

MATERIALS AND METHODS

The use of animals and the procedures employed in this study were approved by the Animal Research Committee of Tottori University (project number: 15-T-47).

Monolayer cell culture

The CMGT SNP cells were established by Osaki et al.[15] and tested for mycoplasma contamination by polymerase chain reaction. SNP cells were seeded in 75-cm^2 cell culture flasks (Corning Inc, Armonk, NY). Adherent SNP cells (2D-SNP cells) were maintained as adherent monolayer cultures in Roswell Park Memorial Institute (RPMI)-1640 medium (Invitrogen; Thermo Fisher Scientific, Inc., Waltham, MA). Subsequently, these cells were supplemented with 10% heat-inactivated fetal bovine serum (FBS; Nichirei Biosciences Inc., Tokyo, Japan) and antibiotics (5 mg/mL penicillin, 5 mg/mL streptomycin, and 10 mg/mL neomycin; Invitrogen; Thermo Fisher Scientific, Inc.) in an atmosphere containing 5% CO_2 at 37°C. The cells were harvested from near-confluent cultures by brief exposure to a solution containing 0.25% w/v trypsin-1 mmol/L ethylenediamine tetraacetic acid-4Na solution with phenol red (FUJIFILM Wako Pure Chemical, Ltd., Osaka, Japan). Trypsinization was stopped using RPMI-1640 medium supplemented with 10% FBS. Cells were concentrated by centrifugation at 300 × *g* for 5 min at 23°C. The cells were resuspended in RPMI-1640 with 10% FBS and transferred to 75-cm^2 cell culture flasks.

Three-dimensional spheroid cell culture

We observed non-adherent SNP cells in the growth medium. SNP spheroids (3D-SNP cells) were established by selecting the non-adherent SNP cells and culturing them without the addition of basement membrane components and ECM-like biomaterials. The cells were concentrated by centrifugation at 300 × *g* for 5 min at 23°C. The cells were resuspended in RPMI-1640 with 10% FBS and transferred to 75-cm^2 cell culture flasks.

miRNA arrays

RNA was extracted from the SNP cells using the miRNeasy mini kit (Qiagen, Venlo, Netherlands), according to the manufacturer's instructions. Extracted total RNA was assessed using a Bioanalyzer (Agilent, CA) and labeled using a 3D-Gene miRNA labeling kit (Toray, Kamakura, Japan). Labeled RNAs were hybridized onto 3D-Gene Human miRNA Oligo chips (Toray, Kamakura, Japan). The annotation and oligonucleotide sequences of the probes conformed to the miRBase Release 21 database (http://microrna.sanger.ac.uk/sequences/). After stringent washes, fluorescent signals were scanned using a 3D-Gene Scanner (Toray Industries) and analyzed using 3D-Gene Extraction software (Toray Industries).

The raw data of each spot were normalized by substitution with the mean intensity of the background signal determined by the signal intensities of all blank spots with 95% confidence intervals. Measurements of spots with signal intensities greater than 2 standard deviations of the background signal intensity were considered valid. The relative expression levels of a given miRNA were calculated by comparing the signal intensities of the valid spots throughout the microarray experiments. The normalized data were globally normalized per array, such that the median of the signal intensity was adjusted to 25.

Morphology

The cell morphology of the 2D monolayer cultures and 3D spheroids was photographed with EVOS XL Cell Imaging Systems (Thermo Fisher Scientific K.K., Tokyo, Japan).

Histopathology of tumor cells

The 2D-SNP cells were fixed in 10% buffered formalin for 24 h and mechanically detached from the bottom of the flask using an IWAKI® cell scraper (AGC Techno Glass Co. LTD, Tokyo, Japan). The 3D-SNP cells were harvested using a plastic pipette and fixed in 10% buffered formalin for 24 h. The 2D- and 3D-SNP cells were embedded in paraffin, cut at a thickness of 4 μm, stained with hematoxylin and eosin (H&E), and examined under a light microscope.

Cell proliferation

The 2D- or 3D-SNP cells were seeded at 1 × 10^3 cells into white 96-well plates (Corning Inc, Armonk, NY) containing 100 μL of culture medium for 24 h. Following incubation, the amount of ATP was determined using KATAMARINO ATP assay reagent ver. 2 (Toyo Benet Co., Ltd., Japan), according to the manufacturer's instructions, for 0 to 48 h each as a cell viability assay. For the standard curve, two-fold serial dilutions of cells were plated, and the readings were taken immediately after seeding. The doubling time at the proliferative phase was calculated using values obtained at 12 and 48 h with the following equation:

Doubling time = Duration/Ln(2)/Ln(Final concentration/Initial concentration)

Tumor models

The use of animals and the procedures employed in this study were approved by the Animal Research Committee of Tottori University (project number: 15-T-47). Six-week-old female NOD/ShiJic-scidJcl mice (CLEA Japan, Tokyo, Japan) were maintained in isolators under specific pathogen-free conditions. All SCID mice were housed and handled under clean conditions using a Jic rack (Jic Co., Kanagawa, Japan) with sterilized water, cages, beddings, and food (CL-2; CLEA Japan). Food and water were provided *ad libitum*. The 2D- and 3D-SNP cells were inoculated subcutaneously into the shaved lower dorsum of mice at a density of 1 × 10^7 cells in 0.1 mL phosphate-buffered saline (PBS) (Nacalai Tesque Inc., Kyoto, Japan) per mouse using a 26-gauge syringe. All mice were sacrificed by cervical dislocation, and the tumors were harvested when the average tumor volume reached approximately 100 mm^3 in the tumor model.

Histopathology of tumor tissues

The harvested tumor tissues were fixed in 10% buffered formalin for 24 h and embedded in paraffin using the routine method. Tumor sections were cut at a thickness of 4 μm, stained with H&E, and examined under a light microscope.

Intracellular concentration of doxorubicin

The 2D- or 3D-SNP cells were seeded at 0.5 × 10^6 cells into a 75 cm^2 tissue culture flask and incubated for 24 h. The cells were incubated with doxorubicin at a final concentration of 4 μM for 4 h at 37°C. The 2D-SNP cells were collected using a cell scraper. The 3D-SNP cells were collected directly. The collected cells were centrifuged at 300 × *g* for 5 min at 23°C and washed with PBS, and the cells were then suspended in radioimmunoprecipitation assay buffer (Nacalai Tesque Inc.) to approximately 1 × 10^6/mL concentration. The cells were lysed using an ultrasonic homogenizer (Branson Sonifier 250, BRANSON Ultrasonics Co., Danbury, CT). The fluorescence of doxorubicin in the lysate of SNP cells was measured using the fluorescence spectrometer SH-9000Lab (excitation wavelength, 470 nm; emission wavelength, 595 nm; Hitachi High-Technologies Co., Tokyo, Japan). In addition, the protein content in the lysate of the SNP cells was measured spectrophotometrically (read at 545 nm) using the TaKaRa BCA Protein Assay Kit (TaKaRa Bio Inc., Shiga, Japan), according to the manufacturer's instructions.

Evaluation of the cytotoxic effects of doxorubicin

The 2D- or 3D-SNP cells were seeded at 1–2 × 10^4 cells/well in 96-well black plates (Corning Costar, Armonk, NY) and incubated for 24 h. The cells were then incubated with various concentrations of doxorubicin (0, 1.5625, 3.125, 6.25, 12.5, 25, or 50 μM) for 24 h at 37°C. The cells were then incubated for 10 min on a hot plate at 37°C using an ATP measurement reagent (KATAMARI ATP Assay reagent; Toyo B-Net Co., Ltd., Tokyo, Japan), according to the manufacturer's instructions. Light intensity was measured using a luminescence microplate reader (LuMate, Awareness Technology Inc., Palm City, FL).

Doxorubicin-induced morphological change

The 2D- or 3D-SNP cells were seeded at 1–2 × 10^5 cells in 35-mm Petri dishes (Thermo Fisher Scientific K.K., Tokyo, Japan) containing 2 mL of cultivation medium for 24 h. Subsequently, the cells were incubated with doxorubicin (4 μM) for 24 h at 37°C. The cells were stained with Hoechst 33342 and examined under a BZ-X810 microscope (Keyence, Osaka, Japan). Images were captured using 360/40 and 460/50 filters (Hoechst 33342) and 560/40 and 630/75 filters (doxorubicin) for excitation and emission, respectively.

Cytotoxicity of echinomycin

The 2D- or 3D-SNP cells were seeded at 1–2 × 10^4 cells/well in 96-well black plates and incubated for 24 h. The cells were then incubated with various concentrations of echinomycin (Abcam, Tokyo, Japan), a hypoxia-inducible factor-1 (HIF-1) DNA-binding activity inhibitor (0, 1. 25, 2.5, 5, or 10 nM), for 8 h at 37°C. The cells were then incubated for 10 min on a hot plate at 37°C using an ATP measurement reagent, according to the manufacturer's instructions.

LOX assay

The 2D- or 3D-SNP cells were seeded at 1–2 × 10^5 cells in 35-mm Petri dishes containing 2 mL of cultivation medium. After 24 h of incubation, the hypoxia probe solution LOX-1® (Medical & Biological Laboratories Co., Ltd., Tokyo, Japan) was incubated at 2 μmol/L with or without echinomycin at 10 nM for 8 h. After washing with a fresh medium, cells were stained with Hoechst 33342. LOX-1 and Hoechst 33342 fluorescence were examined using a BZ-X810 microscope. Images were captured using 360/40 and 460/50 filters (Hoechst 33342) and 560/40 and 630/75 filters (LOX-1) for excitation and emission, respectively.

Table 1. Expression values of microRNAs of SNP cells and reported oncogenic miRNAs of human breast cancer

	SNP cells					Human breast cancer
	Global normalization		Adherent *vs* Sphere			
Name	Adherent	Sphere	Ratio	Log2 ratio	up	Up-regulation
cfa-miR-210	5	52	10.19	3.35	***	Angiogenesis[20, 22] Gene instability[20] Invasion and metastasis[20, 22]
cfa-miR-218	12	112	8.97	3.16	***	Metastasis[30]
cfa-miR-26b	57	230	4.06	2.02	**	Proliferation[20]
cfa-miR-33a	6	26	4.06	2.02	**	
cfa-miR-181b	4	16	3.88	1.96	*	Proliferation[20]
cfa-miR-26a	103	330	3.22	1.68	*	Proliferation[20]
cfa-miR-148a	13	40	3.05	1.61	*	Angiogenesis[20]
cfa-miR-338	10	31	3.02	1.59	*	
cfa-miR-340	6	19	3.00	1.58	*	
cfa-miR-9	19	55	2.93	1.55	*	
cfa-miR-30e	5	15	2.85	1.51	*	
cfa-miR-342	13	36	2.70	1.43	*	
cfa-miR-147	7	17	2.54	1.34	*	
cfa-miR-196a	5	12	2.51	1.33	*	
cfa-miR-374a	4	10	2.50	1.32	*	
cfa-miR-32	3	8	2.43	1.28	*	
cfa-miR-148b	6	14	2.40	1.26	*	
cfa-miR-454	4	8	2.33	1.22	*	
cfa-miR-130a	57	128	2.25	1.17	*	
cfa-miR-429	95	210	2.20	1.14	*	
cfa-miR-138b	7	15	2.14	1.10	*	
cfa-miR-502	4	9	2.06	1.04	*	
cfa-miR-532	3	6	2.06	1.04	*	

*1 > Log2 ratio, **2 > Log2 ratio, ***3 > Log2 ratio

Statistical analyses

Data are presented as the mean ± standard deviation. Unpaired t-tests were used to determine the statistical differences in the intracellular concentration of doxorubicin. The differences between groups were analyzed with a two-way analysis of variance (ANOVA) followed by Sidak's multiple comparison tests, which were used to determine the statistical differences for cell viability in the 2D- and 3D-SNP cells. Differences were considered statistically significant at $P < 0.05$. Statistical analyses were performed using GraphPad Prism software (version 6.0; GraphPad Software, Inc., La Jolla, CA).

RESULTS

miRNA arrays

All samples were analyzed using an Agilent 2100 Bioanalyzer, and the 18S and 28S ribosomal RNA peaks were identified. The RNA integrities of the 2D- and 3D-SNP cells were 9.8 and 9.7, respectively.

A comparison of samples from SNP cells and normal mammary gland tissues revealed 291 different miRNAs. Table 1 lists 23 miRNAs that showed large (> 2-fold) increases in expression in the 3D-SNP cells relative to the 2D-SNP cells. Notably, the miRNA-210 and miRNA-218 expressions showed the largest increase. Table 2 lists 25 miRNAs that showed large (< 0.5-fold) decreases in expression in the 3D-SNP cells relative to the 2D-SNP cells. Notably, the miRNA-708 and miRNA-205 expressions showed the largest decrease.

Table 2. Expression values of microRNAs of SNP cells and reported tumor suppressor miRNAs of human breast cancer

	SNP cells					Human breast cancer
	Global normalization		Adherent *vs* Sphere			
Name	Adherent	Sphere	Ratio	Log2 ratio	Up	Down-regulation
cfa-miR-708	60	9	0.16	–2.67	**	Anti-proliferation[22] Anti-metastasis[21]
cfa-miR-205	170	28	0.16	–2.62	**	Anti-proliferation[21] Anti-metastasis[21]
cfa-miR-206	8	2	0.24	–2.09	**	Anti-proliferation[21] Anti-metastasis[21]
cfa-miR-302c	67	17	0.26	–1.96	*	Anti-proliferation[20]
cfa-miR-487a	11	3	0.26	–1.92	*	
cfa-miR-503	8	2	0.30	–1.72	*	
cfa-miR-184	8	3	0.34	–1.57	*	
cfa-miR-487b	191	65	0.34	–1.56	*	
cfa-miR-139	36	13	0.35	–1.50	*	
cfa-miR-22	82	29	0.36	–1.48	*	
cfa-miR-133c	9	4	0.40	–1.32	*	
cfa-miR-489	21	9	0.42	–1.27	*	
cfa-miR-505	54	23	0.42	–1.24	*	
cfa-miR-10b	5	2	0.43	–1.22	*	
cfa-miR-345	10	4	0.43	–1.22	*	
cfa-miR-483	21	9	0.43	–1.21	*	
cfa-miR-155	54	24	0.44	–1.17	*	
cfa-miR-1307	27	12	0.44	–1.17	*	
cfa-miR-764	9	4	0.46	–1.13	*	
cfa-miR-381	4	2	0.47	–1.08	*	
cfa-miR-494	354	169	0.48	–1.07	*	
cfa-miR-377	4	2	0.48	–1.06	*	Anti-proliferation[20]
cfa-miR-1306	21	10	0.49	–1.04	*	
cfa-miR-365	133	65	0.49	–1.03	*	Anti-proliferation[22]
cfa-miR-326	8	4	0.50	–1.01	*	

*–1 < Log2 ratio, **–2 < Log2 ratio, ***–3 < Log2 ratio

Morphology

In phase-contrast light microscopy images, the 2D-SNP cells displayed epithelial-like cells (Fig. 1A). The 3D-SNP cells displayed round cell conglomerates or spherical aggregates (Fig. 1B).

H&E staining showed that the 2D-SNP cells had clear nuclei with anisokaryosis and prominent nucleoli (Fig. 2A). The cells were arranged in small nests or sheets. In contrast, the 3D-SNP cells were square to cuboidal epithelial-like cells and formed spherical aggregates of cells that randomly adhered to each other. These cells were more uniform in size and shape than the 2D-SNP cells (Fig. 2B).

Cell proliferation

The doubling time at the proliferative phase was calculated between 12 and 48 h (Fig. 3). The doubling times of the 2D- and 3D-SNP cells were 14.7 and 10.7 h, respectively.

Histopathology of tumor tissues

The subcutaneous tumor models of 2D- or 3D-SNP cells were histopathologically assessed. The short and long diameters of 2D- and 3D-SNP tumors were 2.91 ×

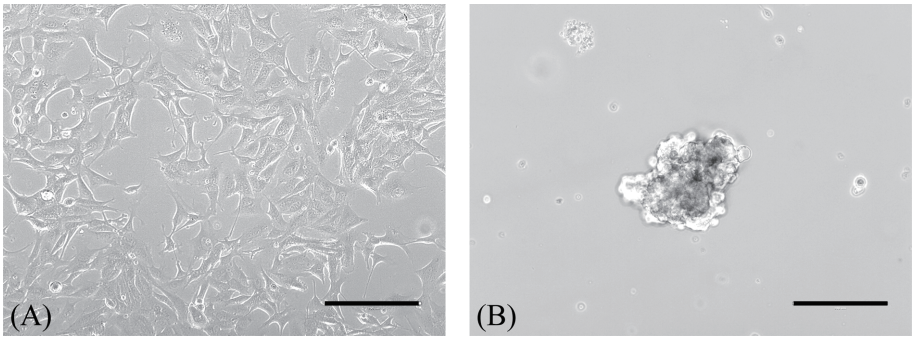

Fig. 1. Morphology of the two-dimensional (2D)- and three-dimensional (3D)-SNP cells. (**A**) The 2D-SNP cells displayed epithelial-like structures. (**B**) The 3D-SNP cells displayed round cell conglomerates. Bar = 100 μm.

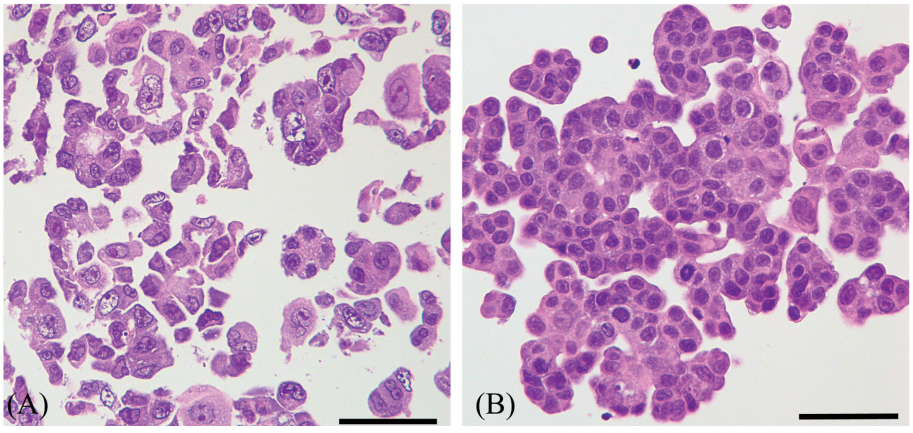

Fig. 2. Histological characterization of the two-dimensional (2D)- and three-dimensional (3D)-SNP cells in vitro. SNP cells were cultured under 2D adherent and 3D spheroid conditions. The 2D- and 3D-SNP cells were stained with hematoxylin and eosin. (**A**) 2D-SNP cells. (**B**) 3D-SNP cells. Bar = 50 μm.

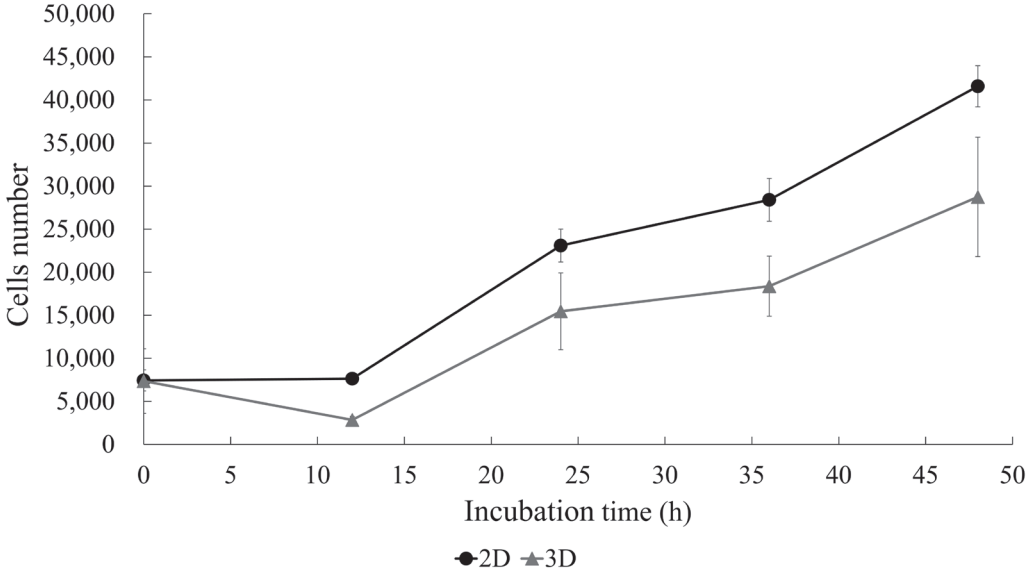

Fig. 3. Cell proliferative growth curves of the two-dimensional (2D)- and three-dimensional (3D)-SNP cells in vitro. Cell proliferation was monitored with the amount of ATP. Data are presented as mean ± standard error.

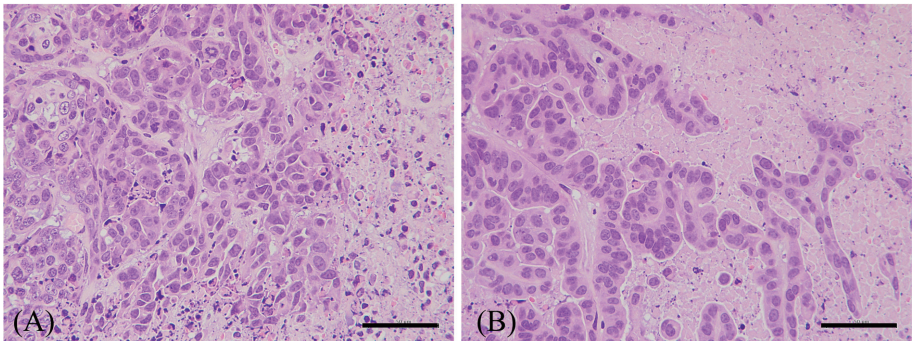

Fig. 4. Histological characterization of the two-dimensional (2D)- and three-dimensional (3D)-SNP cells in vivo. The 2D- or 3D-SNP cells were inoculated subcutaneously into the shaved lower dorsum of NOD/ShiJic-scidJcl mice, and the tumor tissues were stained with hematoxylin and eosin. (**A**) 2D-SNP cells. (**B**) 3D-SNP cells. Bar = 50 µm.

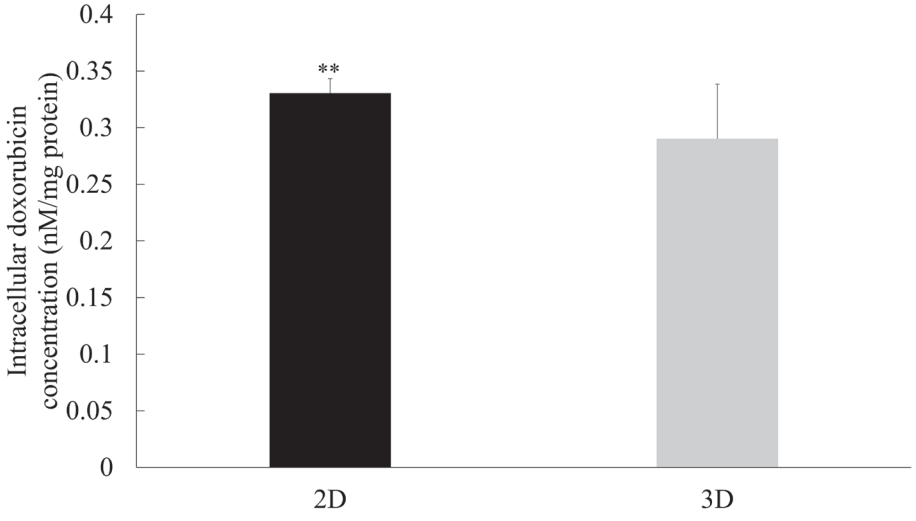

Fig. 5. Intracellular concentration of doxorubicin. Data are presented as mean ± standard deviation. Significant differences are indicated by $^{**}P < 0.01$, unpaired *t*-test; 2D vs 3D ($n = 3$). 2D, two-dimensional; 3D, three-dimensional.

3.97 and 3.71 × 6.79 mm, respectively. The proliferation of 2D-SNP cells showing marked atypia was observed in the mass. These cells were randomly arranged with a thin fibrovascular stroma. Necrotic lesions (right side of the image) and karyokinesis of the cells were also observed (Fig. 4A). In the 3D-SNP cell-grafted mass, cells were ordered in cords or ribbons. Necrosis was also marked within the mass, as observed from the right upper to the center of the image (Fig. 4B).

Intracellular concentration of doxorubicin

The intracellular concentrations of doxorubicin in the 2D- and 3D-SNP cells were 0.330 ± 0.013 and 0.290 ± 0.048 nM/mg protein, respectively (Fig. 5).

Doxorubicin-induced cytotoxicity

Doxorubicin significantly reduced the growth of the 2D- and 3D-SNP cells in a concentration-dependent manner (Fig. 6). The cell viabilities in the 3D-SNP cells treated with 3.125 to 25 µM were significantly lower than those in the 2D-SNP cells ($P < 0.01$). The IC_{50} values of the 2D- or 3D-SNP cells were 5.2 and 1.6 µM, respectively.

Doxorubicin-induced morphological change

To further investigate the effects of doxorubicin on the 2D- or 3D-SNP cells, morphological analysis of cells in the presence or absence of doxorubicin (4 µM) was performed 24 h after treatment (Fig. 7). Hoechst 33342 staining of the 2D-SNP cells untreated with doxorubicin showed no evident morphological changes in the nuclei. The cell density of the 2D-SNP cells treated

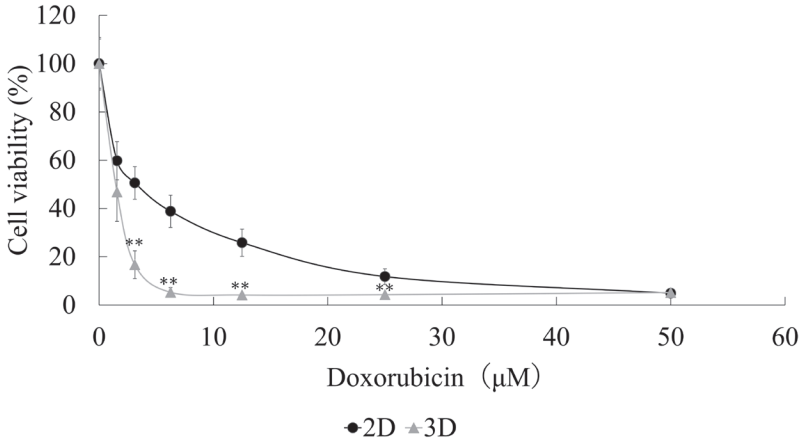

Fig. 6. Cell viabilities in the two-dimensional (2D)- and three-dimensional (3D)-SNP cells. Data are presented as mean ± standard deviation. Significant differences are indicated by $^{**}P < 0.01$, Sidak's multiple comparison test; 2D vs 3D ($n = 6$).

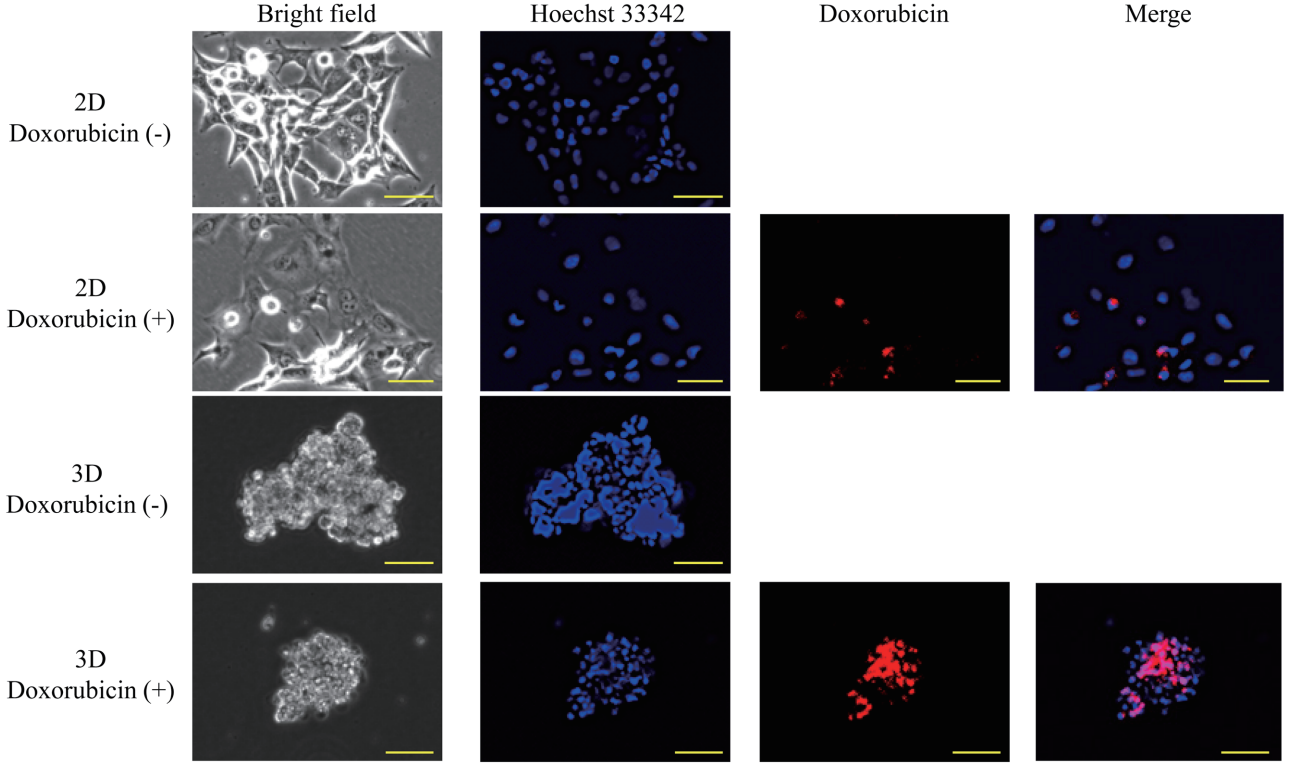

Fig. 7. Doxorubicin-induced morphological changes in the two-dimensional (2D)- and three-dimensional (3D)-SNP cells. Fluorescence microscopy was used to evaluate the morphological changes in the 2D- and 3D-SNP cells. The cells were treated with or without 4 μM doxorubicin for 24 h. The first column represents the phase contrast images, and the consecutive columns represent Hoechst 33342, doxorubicin, and merged images. The nuclei were stained with Hoechst 33342 (blue). Red fluorescence images show intracellular doxorubicin. The merged images contain the blue fluorescence of the nuclei and the red fluorescence of doxorubicin. Bar = 100 μm.

with doxorubicin was lower than that of untreated cells. Hoechst 33342 staining of the 3D-SNP cells treated with doxorubicin showed highly condensed nuclei or fragmented chromatin compared to untreated cells.

Cytotoxicity of echinomycin

Echinomycin is a reversible cell-permeable HIF-1α inhibitor that exhibits potent antitumor activity. Although echinomycin slightly induced cell death, it did not significantly reduce the cell viability of the 2D- or 3D-SNP

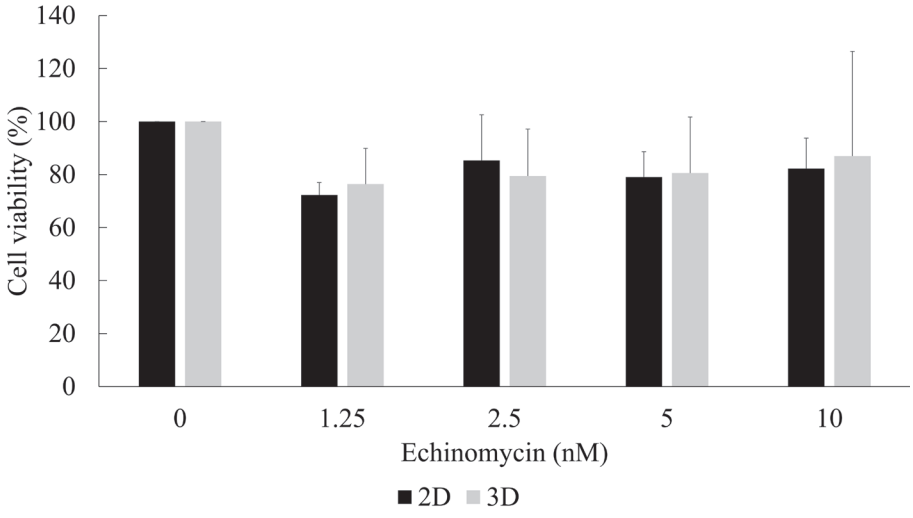

Fig. 8. Cytotoxicity of echinomycin in the two-dimensional (2D)- and three-dimensional (3D)-SNP cells. The cells were treated with 0, 1.25, 2.5, 5, or 10 nM echinomycin for 8 h. Data are presented as mean ± standard deviation. Sidak's multiple comparison test; 2D vs 3D ($n = 3$).

cells in a concentration-dependent manner (Fig. 8). In the LOX assay, the 2D- or 3D-SNP cells were incubated with 10 nM echinomycin.

LOX-1 assay

The oxygen status in the 2D- and 3D-SNP cells was evaluated using the hypoxia probe LOX-1 to detect hypoxic conditions. As shown in Fig. 9, LOX-1 fluorescence was observed inside the spheres of 3D-SNP cells without echinomycin but not in 2D-SNP cells. The 3D-SNP cells treated with echinomycin showed weak LOX-1 fluorescence.

DISCUSSION

The present study compared the characterization in 2D- and 3D-SNP cells. First, we focused on the establishment and characterization of the 3D-SNP cells. In 2D-culture, SNP cells were grown as a monolayer in tissue culture flasks, whereas, in 3D-culture, SNP cells formed spheres of epithelial cells. Our previous study demonstrated that 2D-SNP cells showed tumorigenicity.[15] Similarly, in the present study, 3D-SNP cells exhibited tumorigenicity. Although the morphology of CMGT was histopathologically varied, the tumor tissues derived from 3D-SNP cells maintained the morphology of the epithelial tissues. Moreover, it was similar to the original tumor tissues.[15] There were no differences between 2D-SNP and 3D-SNP cells in malignancy, including the number of mitoses and the degree of necrosis. Additionally, metastasis lesions were not observed in both cells when mice were euthanized.

Second, we performed a chemosensitivity assay using doxorubicin. Traditionally, the efficacy of anticancer drugs has been evaluated in 2D-cultured cancer cell lines. However, it is now considered that culturing cells under 2D conditions is not physiologically relevant. Moreover, 3D-cultured cells possess many features similar to those of solid tumors, such as greater cell proliferation, migration, and chemoresistance, which are not observed in 2D-cultured cells.[16] In the present study, following 24 h incubation of DOX (3.125 to 25 μM), the cell viability in the 3D-SNP cells was significantly decreased compared with the 2D-SNP cells. It was considered that sensitivity to DOX might change by altering the culture conditions. The intracellular DOX concentration in the 2D-SNP cells 4 h after adding DOX at 4 μM was significantly increased compared with the 3D-SNP cells (Fig. 4). However, the fluorescence of DOX in the 3D-SNP cells 24 h after adding DOX at 4 μM was higher than that in the 2D-SNP cells (Fig. 6). This discrepancy might be associated with the chronological changes in membrane permeability induced by DOX. Therefore, it is required to evaluate the cytotoxicity of DOX and intracellular DOX concentration over time.

Third, we evaluated the differences in miRNA expression with miRNA microarrays of 2D- and 3D-SNP cells. In a previous study, 3D-cultured MCF-7 (Michigan Cancer Foundation-7) spheroid cells showed a distinct miRNA expression level compared with that of its parental cells in the 2D condition. The study showed that 25 miRNAs were up-regulated, and 109 miRNAs were down-regulated.[17] Therefore, in this study, we compared the difference in miRNA expression levels between the

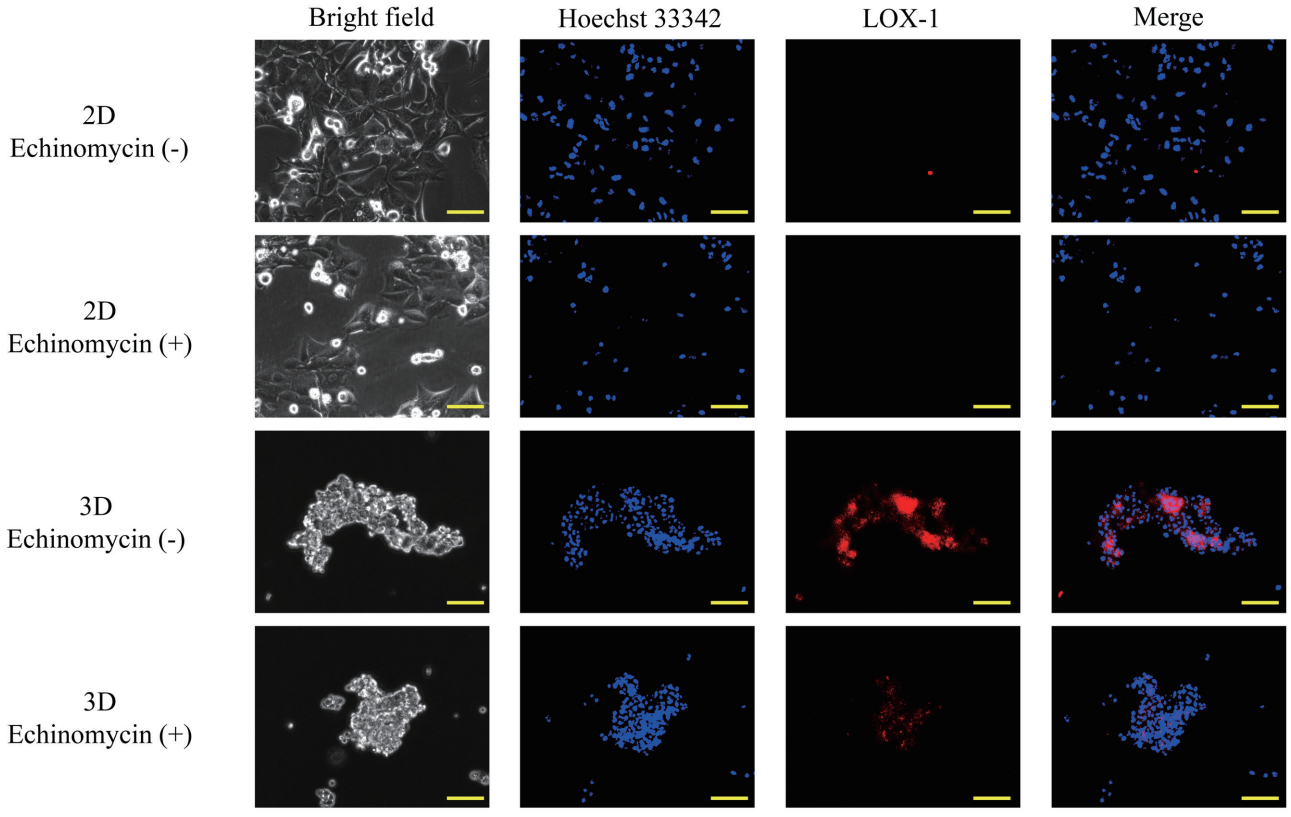

Fig. 9. Hypoxic status in the two-dimensional (2D)- and three-dimensional (3D)-SNP cells. Fluorescence microscopy was used to evaluate the hypoxic status of the 2D- and 3D-SNP cells. The hypoxia probe solution, LOX-1®, was incubated at 2 μmol/L with and without echinomycin at 10 nM for 8 h. The first column represents the phase contrast images, and the consecutive columns represent Hoechst 33342, LOX-1, and merged images. The nuclei were stained with Hoechst 33342 (blue). Red fluorescence images show hypoxic cells. The merged images contain the blue fluorescence of the nuclei and red fluorescence of LOX-1. Bar = 100 μm.

2D- and 3D-SNP cells. The expression of miRNA-210 in the 3D-SNP cells was 10.19 times higher than that in the 2D-SNP cells, and the overexpression of miR-210 regulated the proliferation, migration, and apoptosis in breast cancer cells.[18–22] Moreover, high plasma expression levels of miR-210 were associated with tumor presence in patients with breast cancer.[23] Therefore, the overexpression of miR-210 in breast cancer is correlated with a poor prognosis.

Moreover, miR-210 expression increased under hypoxia in canine glioma and melanoma.[24, 25] Fluorescence of the hypoxia probe, LOX-1, was observed in 3D-SNP cells but not in 2D-SNP cells. Hypoxia in the 3D environment of tumors induced the stable expression of HIF-1.[26] In vivo, HIF-1 promotes various cancer progression, including angiogenesis, cell motility, metabolic reprogramming, and resistance to radiation therapy and chemotherapy.[26, 27] In this study, we used echinomycin, an inhibitor of HIF-1 DNA-binding. It is a cyclic peptide belonging to a family of quinoxaline antibiotics isolated from *Streptomyces echinatus*.[28, 29] Fluorescence of LOX-1 in 3D-SNP cells was not observed after co-culture with echinomycin. Therefore, there was a hypoxic area in the 3D-SNP cells, and HIF-1 DNA-binding activity in 3D-SNP cells was inhibited by echinomycin. In the future, various assays after co-incubation of 3D-SNP cells with echinomycin might be required to elucidate the tumor dynamics and develop the treatment for tumor associated with hypoxia.

The size and metastasis of tumors in miR-210-knockdown breast cancer BCF-7 spheroid cells were significantly smaller than those in control spheroid cells.[19] In a previous report, miR-210 was significantly overexpressed in CMGT tissues compared with normal mammary gland tissues.[9] Therefore, the inhibition of miR-210 might serve as an efficient strategy in antitumor gene therapy.

The expression of miRNA-218 in 3D-SNP cells was 8.97 times higher than that in 2D-SNP cells. Circulating miR-218 is associated with breast cancer metastasis.[30] Thus, miR-218 may serve as a diagnostic

and/or prognostic marker for breast cancer. In contrast, miR-218 acts as a tumor suppressor and modulator of drug responses via survival in breast cancer.[31] The intracellular concentration of DOX in the 3D-SNP cells was not higher than that in the 2D-SNP cells. However, in the cytotoxicity assay using DOX, the 3D-SNP cells were more sensitive to DOX than the 2D-SNP cells. The discrepancy between intracellular DOX concentration and cell survival rate might be correlated with the overexpression of miR-218.

Contrarily, the expression of miRNA-708 and miRNA-205 in the 3D-SNP cells was lower than in the 2D-SNP cells. However, these miRNA act as both tumor suppressors[32–34] and oncogenes, contributing to disease progression[35, 36] depending on cell and tumor types. Therefore, the mechanism of these miRNAs requires further study in SNP cells.

In conclusion, the present study showed a clear difference in miRNA expression levels in cells cultured in a 2D adherent versus a 3D spheroid model. As shown in Tables 1 and 2, increased miRNAs in 3D-SNP cells were associated with oncogenic miRNAs. Conversely, decreased miRNAs in 3D-SNP cells were associated with tumor suppressor miRNAs. Moreover, the hypoxic conditions of 3D-SNP cells also significantly differed from those of 2D-SNP cells. 3D cell culture might imitate the *in vivo* behavior of SNP cells within tumor tissues, as reported in human breast cancers. Therefore, the present study suggests that the 3D culture model is superior to traditional 2D adherent cultures in in vitro CMGT research.

Acknowledgments: We would like to thank Editage (www.editage.jp) for English language editing. We also would like to thank Mr. Satoshi Kondo, who is an employee of Toray Industries, for the miRNA array analysis.

The authors declare no conflicts of interest.

REFERENCES

1 Sorenmo KU, Worley DR, Zappulli V. Tumors of the mammary gland. In: Withrow SJ, Vail DM, editors. Withrow and MacEwen's small animal clinical oncology 6th ed.-Saint Louis: Elsevier Saunders; 2020. p. 604-25.
2 Gray M, Meehan J, Martínez-Pérez C, Kay C, Turnbull AK, Morrison LR, et al. Naturally-occurring canine mammary tumors as a translational model for human breast cancer. Front Oncol. 2020;10:617. DOI: 10.3389/fonc.2020.00617, PMID: 32411603
3 von Euler H. Tumours of the mammary glands. In: Dobson JM, Las celles BDX, editors. BSAVA manual of canine and feline oncology 3rd ed. Gloucester: British Small Animal Veterinary Association; 2011. p. 237-47.
4 Dexheimer PJ, Cochella L. MicroRNAs: from mechanism to organism. Front Cell Dev Biol. 2020;8:409. DOI: 10.3389/fcell.2020.00409, PMID: 32582699
5 Adhami M, Haghdoost AA, Sadeghi B, Malekpour Afshar R. Candidate miRNAs in human breast cancer biomarkers: a systematic review. Breast Cancer. 2018;25:198-205. DOI: 10.1007/s12282-017-0814-8, PMID: 29101635
6 Fridrichova I, Zmetakova I. MicroRNAs contribute to breast cancer invasiveness. Cells. 2019;8:1361. DOI: 10.3390/cells8111361, PMID: 31683635
7 Nurzadeh M, Naemi M, Sheikh Hasani S. A comprehensive review on oncogenic miRNAs in breast cancer. J Genet. 2021;100:15. DOI: 10.1007/s12041-021-01265-7, PMID: 33764337
8 Boggs RM, Wright ZM, Stickney MJ, Porter WW, Murphy KE. MicroRNA expression in canine mammary cancer. Mamm Genome. 2008;19:561-9. DOI: 10.1007/s00335-008-9128-7, PMID: 18665421
9 von Deetzen MC, Schmeck BT, Gruber AD, Klopfleisch R. Malignancy associated microRNA expression changes in canine mammary cancer of different malignancies. ISRN Vet Sci. 2014;2014:1-5. DOI: 10.1155/2014/148597, PMID: 25002976
10 Bulkowska M, Rybicka A, Senses KM, Ulewicz K, Witt K, Szymanska J, et al. MicroRNA expression patterns in canine mammary cancer show significant differences between metastatic and non-metastatic tumours. BMC Cancer. 2017;17:728. DOI: 10.1186/s12885-017-3751-1, PMID: 29115935
11 Riaz M, van Jaarsveld MTM, Hollestelle A, Prager-van der Smissen WJC, Heine AAJ, Boersma AWM, et al. miRNA expression profiling of 51 human breast cancer cell lines reveals subtype and driver mutation-specific miRNAs. Breast Cancer Res. 2013;15:R33. DOI: 10.1186/bcr3415, PMID: 23601657
12 Hua B, Li Y, Yang X, Niu X, Zhao Y, Zhu X. MicroRNA-361-3p promotes human breast cancer cell viability by inhibiting the E2F1/P73 signalling pathway. Biomed Pharmacother. 2020;125:109994. DOI: 10.1016/j.biopha.2020.109994, PMID: 32092817
13 Kapałczyńska M, Kolenda T, Przybyła W, Zajączkowska M, Teresiak A, Filas V, et al. 2D and 3D cell cultures - a comparison of different types of cancer cell cultures. Arch Med Sci. 2018;14:910-9. PMID: 30002710
14 Ryan SL, Baird AM, Vaz G, Urquhart AJ, Senge, Richard DJ, et al. Drug discovery approaches utilizing three-dimensional cell culture. Assay Drug Dev Technol. 2016;14:19-28. DOI: 10.1089/adt.2015.670, PMID: 26866750
15 Osaki T, Sunden Y, Sugiyama A, Azuma K, Murahata Y, Tsuka T, et al. Establishment of a canine mammary gland tumor cell line and characterization of its miRNA expression. J Vet Sci. 2016;17:385-90. DOI: 10.4142/jvs.2016.17.3.385, PMID: 26726024
16 Imamura Y, Mukohara T, Shimono Y, Funakoshi Y, Chayahara N, Toyoda M, et al. Comparison of 2D- and 3D-culture models as drug-testing platforms in breast cancer. Oncol Rep. 2015;33:1837-43. DOI: 10.3892/or.2015.3767, PMID: 25634491
17 Boo L, Ho WY, Ali NM, Yeap SK, Ky H, Chan KG, et al. MiRNA transcriptome profiling of spheroid-enriched cells with cancer stem cell properties in human breast MCF-7 Cell Line. Int J Biol Sci. 2016;12:427-45. DOI: 10.7150/ijbs.12777, PMID: 27019627
18 Ivan M, Huang X. miR-210: fine-tuning the hypoxic response. Adv Exp Med Biol. 2014;772:205-27. DOI: 10.1007/978-1-4614-5915-6_10, PMID: 24272361

19 Lan Y, Niu H, Wang H, Yang Z, Cui Z, Jiang J. HIF-1α regulates miR-210 to affect biological behavior of breast cancer cells. Int J Clin Exp Pathol. 2016;9:11487-92.
20 Bertoli G, Cava C, Castiglioni I. MicroRNAs: New Biomarkers for Diagnosis, Prognosis, Therapy Prediction and Therapeutic Tools for Breast Cancer. Theranostics. 2015;5:1122-43. DOI: 10.7150/thno.11543, PMID: 26199650
21 Kaboli PJ, Rahmat A, Ismail P, Ling KH. MicroRNA-based therapy and breast cancer: A comprehensive review of novel therapeutic strategies from diagnosis to treatment. Pharmacol Res. 2015;97:104-21. DOI: 10.1016/j.phrs.2015.04.015, PMID: 25958353
22 Loh HY, Norman BP, Lai KS, Rahman NMANA, Alitheen NBM, Osman MA. The Regulatory Role of MicroRNAs in Breast Cancer. Int J Mol Sci. 2019;20:4940. DOI: 10.3390/ijms20194940, PMID: 31590453
23 Jung EJ, Santarpia L, Kim J, Esteva FJ, Moretti E, Buzdar AU, et al. Plasma microRNA 210 levels correlate with sensitivity to trastuzumab and tumor presence in breast cancer patients. Cancer. 2012;118:2603-14. DOI: 10.1002/cncr.26565, PMID: 22370716
24 Koehler J, Sandey M, Prasad N, Levy SA, Wang X, Wang X. Differential Expression of miRNAs in Hypoxia ("HypoxamiRs") in Three Canine High-Grade Glioma Cell Lines. Front Vet Sci. 2020;7:104. DOI: 10.3389/fvets.2020.00104, PMID: 32258065
25 Hino Y, Rahman MM, Lai YC, Husna AA, Chen H, Hasan MN, et al. Hypoxic miRNAs expression are different between primary and metastatic melanoma cells. Gene. 2021;782:145552. DOI: 10.1016/j.gene.2021.145552, PMID: 33705812
26 Riffle S, Hegde RS. Modeling tumor cell adaptations to hypoxia in multicellular tumor spheroids. J Exp Clin Cancer Res. 2017;36:102. DOI: 10.1186/s13046-017-0570-9, PMID: 28774341
27 Wicks EE, Semenza GL. Hypoxia-inducible factors: cancer progression and clinical translation. J Clin Invest. 2022;132:e159839. DOI: 10.1172/JCI159839, PMID: 35642641
28 Waring MJ, Wakelin LPG. Echinomycin: a bifunctional intercalating antibiotic. Nature. 1974;252:653-7. DOI: 10.1038/252653a0, PMID: 4437614
29 Kong D, Park EJ, Stephen AG, Calvani M, Cardellina JH, Monks A, et al. Echinomycin, a small-molecule inhibitor of hypoxia-inducible factor-1 DNA-binding activity. Cancer Res. 2005;65:9047-55. DOI: 10.1158/0008-5472.CAN-05-1235, PMID: 16204079
30 Liu X, Cao M, Palomares M, Wu X, Li A, Yan W, et al. Metastatic breast cancer cells overexpress and secrete miR-218 to regulate type I collagen deposition by osteoblasts. Breast Cancer Res. 2018;20:127. DOI: 10.1186/s13058-018-1059-y, PMID: 30348200
31 Hu Y, Xu K, Yagüe E. miR-218 targets survivin and regulates resistance to chemotherapeutics in breast cancer. Breast Cancer Res Treat. 2015;151:269-80. DOI: 10.1007/s10549-015-3372-9, PMID: 25900794
32 Saini S, Yamamura S, Majid S, Shahryari V, Hirata H, Tanaka Y, et al. MicroRNA-708 induces apoptosis and suppresses tumorigenicity in renal cancer cells. Cancer Res. 2011;71:6208-19. DOI: 10.1158/0008-5472.CAN-11-0073, PMID: 21852381
33 Guo P, Lan J, Ge J, Nie Q, Mao Q, Qiu Y. miR-708 acts as a tumor suppressor in human glioblastoma cells. Oncol Rep. 2013;30:870-6. DOI: 10.3892/or.2013.2526, PMID: 23754151
34 Gandellini P, Folini M, Longoni N, Pennati M, Binda M, Colecchia M, et al. miR-205 Exerts tumor-suppressive functions in human prostate through down-regulation of protein kinase Cepsilon. Cancer Res. 2009;69:2287-95. DOI: 10.1158/0008-5472.CAN-08-2894, PMID: 19244118
35 Jang JS, Jeon HS, Sun Z, Aubry MC, Tang H, Park CH, et al. Increased miR-708 expression in NSCLC and its association with poor survival in lung adenocarcinoma from never smokers. Clin Cancer Res. 2012;18:3658-67. DOI: 10.1158/1078-0432.CCR-11-2857, PMID: 22573352
36 He L, Zhu W, Chen Q, Yuan Y, Wang Y, Wang J, et al. Ovarian cancer cell-secreted exosomal miR-205 promotes metastasis by inducing angiogenesis. Theranostics. 2019;9:8206-20. DOI: 10.7150/thno.37455, PMID: 31754391